

Robust d-wave pairing symmetry in multi-orbital cobalt high temperature superconductors

Yinxiang Li,^{1,*} Xinloong Han,^{1,*} Shengshan Qin,¹ Congcong Le,¹ Qiang-Hua Wang,^{2,3} and Jiangping Hu^{1,4,5,†}

¹*Beijing National Laboratory for Condensed Matter Physics,
and Institute of Physics, Chinese Academy of Sciences, Beijing 100190, China*

²*National Laboratory of Solid State Microstructures and School of Physics, Nanjing University, Nanjing, 210093, China*

³*Collaborative Innovation Center of Advanced Microstructures, Nanjing University, Nanjing, 210093, China*

⁴*Collaborative Innovation Center of Quantum Matter, Beijing, China*

⁵*Kavli Institute of Theoretical Sciences, University of Chinese Academy of Sciences, Beijing, 100190, China*

(Dated: July 31, 2021)

The pairing symmetry of the newly proposed cobalt high temperature (high- T_c) superconductors formed by vertex shared cation-anion tetrahedral complexes is studied by the methods of mean field, random phase approximation (RPA) and functional renormalization group (FRG) analysis. The results of all these methods show that the $d_{x^2-y^2}$ pairing symmetry is robustly favored near half filling. The RPA and FRG methods, which are valid in weak interaction regions, predict that the superconducting state is also strongly orbital selective, namely the $d_{x^2-y^2}$ orbital that has the largest density near half filling among the three t_{2g} orbitals dominates superconducting pairing. These results suggest that the new materials, if synthesized, can provide indisputable test to high- T_c pairing mechanism and the validity of different theoretical methods.

I. INTRODUCTION

Since the discovery of high temperature (high- T_c) superconductors, cuprates¹ and iron-based superconductors², searching for new high T_c superconductors and explaining their pairing mechanism become crucial tasks in condensed matter physics. However, as the pairing mechanism still remains illusive, few useful theoretical clues have been provided to predict or identify new high- T_c materials.

Recently, through extensive analysis of theoretical and experiment results, some of us have suggested that the two known high T_c families share a common electronic property—those d orbitals with the strongest in-plane $d-p$ coupling in the cation-anion complex are isolated near Fermi energy³⁻⁵. From the viewpoint of magnetically-driven superconducting mechanism, this property implies that the effective antiferromagnetic (AFM) superexchange interaction is the underlining driven force of high T_c superconductivity. Moreover, this crucial property is largely absent in other correlated electronic systems. Thus, the uniqueness of this electronic structure suggests that it can be the key to predict or identify possible high T_c materials. Finding a new family of high T_c materials with the common electronic structure can provide a convincing test to superconducting pairing mechanism.

Following the above theoretical guide, two explicit proposals have been made for Co/Ni transition metal compounds as potential candidates for high T_c superconductors^{3,6}. The first one includes a two dimensional hexagonal lattice formed by edge-shared trigonal bipyramidal complexes³ and the second one hosts a two dimensional square lattice formed by vertex-shared tetrahedra complexes⁶. In both cases, a d^7 filling configuration meets the required electronic condition to be a potential high T_c material.

The second proposal is particularly interesting because it provides an explicit playground to bridge and unify iron-based superconductors and cuprates. On the one hand, the square lattice formed by vertex-shared tetrahedra complexes is similar to the one formed by vertex-shared octahedra complexes in cuprates. Based on the empirical Hu-Ding principle⁷ of the pairing symmetry selection based on the matching between the pairing form factors from the AFM superexchange interactions and Fermi surfaces, we can easily argue that a superconducting state with a d-wave pairing symmetry is favored. On the other hand, similar to those of iron-based superconductors, the electronic structure is attributed to the multi t_{2g} orbitals. Those antiferromagnetic superexchange couplings, similar to those iron-based superconductors that are responsible for superconductivity, are maintained. Although the proposal structure has not been synthesized experimentally, the square CoA_2 ($A=\text{S,Se}$) lattice can be theoretically constructed through the well known cubic Zinc-Blende structure. For example, using MBE (Molecular beam epitaxy), we may grow ZnCoS_2 ⁶ which hosts layered square lattices with vertex-shared CoS_4 tetrahedra by replacing half of Zn atoms in ZnS by Co⁶.

In this paper, we carry out a systematic investigation of the superconducting state in this family of materials under a variety of theoretical methods, including the mean field approach, random phase approximation (RPA) and functional renormalization groups (FRG). All these methods show that the d-wave pairing symmetry is robustly favored in this system while the pairing strength among different t_{2g} orbitals depends on theoretical methods. In particular, as the RPA and FRG methods are very sensitive to the density of states near Fermi energy, both methods predict that the superconducting state is strongly orbital selective. The $d_{x^2-y^2}$ orbital that has the largest density near half filling among the three t_{2g} orbitals dominates superconducting pairing within the

reasonable range of the interaction parameters.

The paper is organized as follows. In Sec. II, we present the mean field analysis of the effective $t-J$ model to show the pairing symmetry near the half filling regime. We find that the $d_{x^2-y^2}$ wave pairing from d_{xz} and d_{yz} orbitals is competing with that from $d_{x^2-y^2}$ orbital. In Sec. III, we provide the gap function within three-orbital Hubbard model by RPA method. The symmetry of $d_{x^2-y^2}$ wave is always the largest pairing strength which mainly from the contribution of $d_{x^2-y^2}$ orbital electrons. In Sec. IV, we find the full pockets have d -wave pairing symmetry by FRG analysis. The pairing form factor mainly situates at the β pocket, showing a very strong $d_{x^2-y^2}$ orbital selection when the system is doped near the half filling. Finally, we summarize and discuss these results in Sec. V.

II. THE MEAN FIELD RESULTS FROM THE MULTI-ORBITAL T-J MODEL

We use the model that is derived for the single layer CoS₂ in the ZnCoS₂ compound⁶. Since only the three t_{2g} orbitals appear near the Fermi level and the nearest neighbour (NN) antiferromagnetic (AFM) interaction is responsible for superconductivity (SC)⁶, the following calculations are all done based on the three bands model in ref. 6 with the NN AFM interaction J . The tight-binding model is given in ref. 6 as

$$H_0 = \begin{pmatrix} H_{11} - \mu & H_{12} & H_{13} \\ H_{21} & H_{22} - \mu & H_{23} \\ H_{31} & H_{32} & H_{33} - \mu \end{pmatrix}. \quad (1)$$

The elements of H_0 matrix are given by⁶

$$\begin{aligned} H_{11} &= \epsilon_1 + 2t_x^{11} \cos(k_x) + 2t_y^{11} \cos(k_y) + 4t_{xy}^{11} \cos(k_x) \cos(k_y) \\ &\quad + 2t_{xx}^{11} \cos(2k_x) + 2t_{yy}^{11} \cos(2k_y), \\ H_{12} &= -4t_{xy}^{12} \sin(k_x) \sin(k_y) \\ H_{13} &= 2it_x^{13} \sin(k_x) + 4it_{xy}^{13} \sin(k_x) \cos(k_y) + 2it_{xx}^{13} \sin(2k_x) \\ H_{22} &= \epsilon_2 + 2t_x^{22} \cos(k_x) + 2t_y^{22} \cos(k_y) + 4t_{xy}^{22} \cos(k_x) \cos(k_y) \\ &\quad + 2t_{xx}^{22} \cos(2k_x) + 2t_{yy}^{22} \cos(2k_y), \\ H_{23} &= 2it_y^{23} \sin(k_y) + 4it_{xy}^{23} \sin(k_y) \cos(k_x) + 2it_{xx}^{23} \sin(2k_y) \\ H_{33} &= \epsilon_3 + 2t_x^{33} (\cos(k_x) + \cos(k_y)) + 4t_{xy}^{33} \cos(k_x) \cos(k_y) \\ &\quad + 2t_{xx}^{33} (\cos(2k_x) + \cos(2k_y)). \end{aligned} \quad (2)$$

Without a further specification, we take all energy parameters in the unit of eV. In above equation, $\epsilon_1 = \epsilon_2 = 3.7314$ and $\epsilon_3 = 4.1241$ are the onset energy of $d_{xz,yz}$ and $d_{x^2-y^2}$. The corresponding hopping parameters are $t_x^{11} = t_y^{22} = 0.4391$, $t_y^{11} = t_x^{22} = 0.1408$, $t_{xy}^{11} = t_{xy}^{22} = -0.0162$, $t_{xy}^{12} = 0.021$, $t_x^{13} = t_y^{23} = 0.0057$, $t_{xy}^{13} = t_{xy}^{23} = -0.0061$, $t_x^{33} = 0.1824$, $t_{xy}^{33} = 0.011$, $t_{xx}^{11} = t_{yy}^{22} = 0.0688$, $t_{yy}^{11} = t_{xx}^{22} = -0.0025$, $t_{xx}^{13} = t_{yy}^{23} = 0.0107$, $t_{xx}^{33} = -0.0299$, in which $x(y)$ labels the hopping between

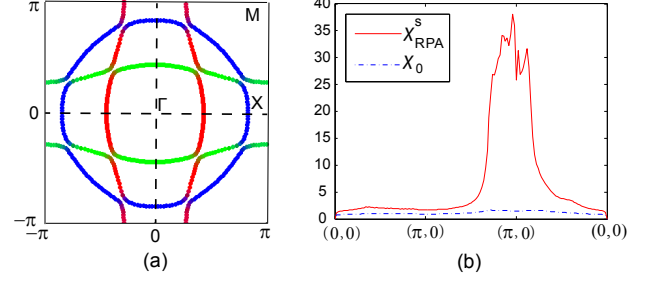


FIG. 1: (color online) The orbital contributions of the different FS sheets are shown color coded: d_{xz} (red), d_{yz} (green) and $d_{x^2-y^2}$ (blue) at the 0.5 electron doping with respect to the half filling in (a). The bare susceptibility and RPA spin susceptibility with $U = 0.48$ and $J_H/U = 0.2$ in (b).

two NN sites along x (y) directions, xy labels the hopping between two next NN sites, and xx (yy) labels the hopping between two third NN sites along x (y) directions. The Fermi surface (FS) of three-orbital model is plotted in Fig. 1(a) with 0.5 electron doped per site away from half filling. The Fermi surface includes two hole pockets around the Γ point and one electron pocket around the M point in the first Brillouin zone (BZ). In the spirit of the $t-J$ model, the kinetic energy is also subject to a full suppression of on-site double occupancy. In the mean field calculation, we can absorb this suppression into an effective overall renormalization factor of the bare band structure^{8,9}. In general, this renormalization factor is also doping dependent. As here we focus on qualitatively obtaining the pairing symmetry, we can simply stick to the bare band structure by rescaling the interaction parameters.

Now, we consider the effective AFM interactions in this family. The effective AFM interactions are generated by the superexchange process. Moreover, the intra-orbital AFM couplings dominate over the inter-orbital AFM couplings. The intra-orbital AFM couplings can be estimated as

$$J_\alpha = 4t_{eff,\alpha}^2 \left(\frac{1}{U_d} + \frac{1}{U_d + \Delta_{pd}} \right), \quad (3)$$

where U_d is the Coulomb interaction for the d_α orbital, $t_{eff,\alpha} = t_{pd,\alpha}^2 / (U_d + \Delta_{pd})$ is the effective intra-orbital hopping between the d_α orbitals at two NN sites and $\Delta_{pd} = \epsilon_d - \epsilon_p$ is the energy difference between the d_α orbital and p orbital. The hopping parameters and onsite energy for p and d_α orbitals can be obtained by DFT calculation⁶ and the Coulomb interaction for the d orbitals U_d is set to be $3.0eV$ ⁶. After detailed calculations from DFT results, we found that for the $d_{x^2-y^2}$ orbital, $J_{x^2-y^2} \sim 0.07$. For the d_{xz} and d_{yz} orbitals, the couplings are different along the two different direction so that we denote them as $J_{xz}^x = J_{yz}^y \sim 0.25$ and $J_{xz}^y = J_{yz}^x \sim 0.03$. In the following, we fix the ratio between different J_α according to these estimation values in our calculation and vary them by multiplying a single interaction scaling pa-

parameter J . The value of J can be viewed as the renormalization factor of the bare band from the electron-electron correlation.

We can use the standard mean field method to decouple the AFM interaction in the superconducting channel. The superconducting order parameters in the spin singlet pairing channel are defined as

$$\Delta_{\langle rr' \rangle, \alpha} = J_{\alpha} \langle c_{\alpha, r, \uparrow} c_{\alpha, r', \downarrow} - c_{\alpha, r, \downarrow} c_{\alpha, r', \uparrow} \rangle, \quad (4)$$

where $\langle rr' \rangle$ represents two NN sites and $c_{\alpha, r, \sigma}$ are Fermionic operators. In a uniform superconducting state, the superconducting order parameters are also translation invariant. Considering the three t_{2g} orbitals, we have six independent pairing order parameters, Δ_{α}^a with a denoting the directions and α denoting orbitals. Since the lattice equivalently has the D_{4h} symmetry by a gauge transformation, the order parameters can form two one-dimensional irreducible representations, namely, a s-wave pairing (A_{1g}) state and a d-wave pairing (B_{1g}) state, as follows,

$$\begin{aligned} \Delta_1^s &= (\Delta_{xz}^x + \Delta_{yz}^y)/2, \\ \Delta_1^d &= (\Delta_{xz}^x - \Delta_{yz}^y)/2, \\ \Delta_2^s &= (\Delta_{xz}^y + \Delta_{yz}^x)/2, \\ \Delta_2^d &= (\Delta_{xz}^y - \Delta_{yz}^x)/2, \\ \Delta_3^s &= (\Delta_{x^2-y^2}^x + \Delta_{x^2-y^2}^y)/2, \\ \Delta_3^d &= (\Delta_{x^2-y^2}^x - \Delta_{x^2-y^2}^y)/2. \end{aligned} \quad (5)$$

Among these six order parameters, $\Delta_2^{s,d}$ are much smaller than the others because the $d-p$ couplings for the $d_{xz, yz}$ orbitals along the corresponding directions are very small. Therefore, we ignore $\Delta_2^{s,d}$ in the following calculations. In the momentum space, the mean-field Hamiltonian can be written as

$$H = \begin{pmatrix} H_0(k) & \Delta(k) \\ \Delta^\dagger(k) & -H_0^*(-k) \end{pmatrix}, \quad (6)$$

where

$$\Delta(k) = \begin{pmatrix} \Delta_{11}(k) & 0 & 0 \\ 0 & \Delta_{22}(k) & 0 \\ 0 & 0 & \Delta_{33}(k) \end{pmatrix}, \quad (7)$$

and

$$\begin{aligned} \Delta_{11}(k) &= (\Delta_1^s + \Delta_1^d) \cos(k_x) \\ \Delta_{22}(k) &= (\Delta_1^s - \Delta_1^d) \cos(k_y) \\ \Delta_{33}(k) &= \Delta_3^s (\cos(k_x) + \cos(k_y)) \\ &\quad + \Delta_3^d (\cos(k_x) - \cos(k_y)). \end{aligned} \quad (8)$$

By fixing the ratio between different AFM interactions, we can calculate the mean-field phase diagram for the pairing symmetry with respect to a single interaction scaling parameter J . The result is shown in the Fig. 2(a). The most favored pairing symmetry is the

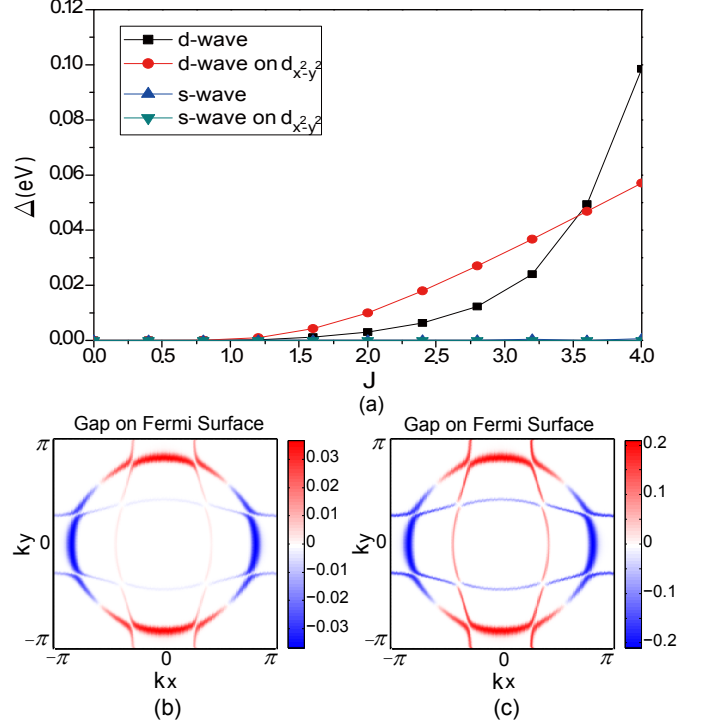


FIG. 2: (color online) The mean field phase diagram with NN antiferromagnetic parameter J in (a). The $d_{x^2-y^2}$ -wave pairing symmetry with $J = 2.0$ in (b) and $J = 4.0$ in (c).

d wave within all parameter ranges. The contribution from the d_{xz} and d_{yz} orbitals increases significantly when J increases. When J is less than 3.5, the d -wave pairing on the $d_{x^2-y^2}$ orbital which has the geometric factor $\cos(k_x) - \cos(k_y)$ is stronger than those on the other two orbitals. When J is larger than 3.5, the d -wave pairing on d_{xz} and d_{yz} orbitals becomes stronger. The SC gap on the Fermi surfaces (FSs) are shown in Fig. 2(b) and (c) when $J = 2.0$ and $J = 4.0$. There are SC gap nodes along the (π, π) direction.

III. RANDOM PHASE APPROXIMATION ANALYSIS

In this section, we perform calculations under the RPA approximation to obtain the pairing symmetry under the standard spin-fluctuation mechanism. The full Hamiltonian used in the following calculation is

$$\begin{aligned} H &= H_0 + U \sum_{i, \alpha} n_{i\alpha\uparrow} n_{i\alpha\downarrow} + U' \sum_{i, \alpha < \beta} n_{i\alpha} n_{i\beta} \\ &\quad + J_H \sum_{i, \alpha < \beta, \sigma \sigma'} c_{i\alpha\sigma}^\dagger c_{i\beta\sigma'}^\dagger c_{i\alpha\sigma'} c_{i\beta\sigma} \\ &\quad + J' \sum_{i, \alpha \neq \beta} c_{i\alpha\uparrow}^\dagger c_{i\alpha\downarrow}^\dagger c_{i\beta\downarrow} c_{i\beta\uparrow}, \end{aligned} \quad (9)$$

where H_0 is the above tight binding three bands model and $n_{i,\alpha} = n_{i,\alpha,\uparrow} + n_{i,\alpha,\downarrow}$. For other indexes, we adopt the parameter notations given in ref. 10. In the RPA approximation, the pairing vertex is

$$\Gamma_{ij}(k, k') = \text{Re} \left[\sum_{l_1 l_2 l_3 l_4} a_{v_i}^{l_2,*}(k) a_{v_i}^{l_3,*}(-k) \right. \\ \left. \times \Gamma_{l_1 l_2 l_3 l_4}(k, k', \omega = 0) a_{v_j}^{l_1}(k') a_{v_j}^{l_4}(-k') \right], \quad (10)$$

where the momenta k and k' is restricted to different FSs with $k \in C_i$ and $k' \in C_j$. a_v^l (orbital index l and band index v) is the component of the eigenvectors of the three-orbital tight binding Hamiltonian. The singlet channel of orbital vertex function $\Gamma_{l_1 l_2 l_3 l_4}$ in RPA is given by

$$\Gamma_{l_1 l_2 l_3 l_4}(k, k', \omega) = \left[\frac{3}{2} \bar{U}^s \chi_1^{RPA}(k - k', \omega) \bar{U}^s + \frac{1}{2} \bar{U}^s \right. \\ \left. - \frac{1}{2} \bar{U}^c \chi_0^{RPA}(k - k', \omega) \bar{U}^c + \frac{1}{2} \bar{U}^c \right]_{l_3 l_4 l_1 l_2}, \quad (11)$$

where χ_1^{RPA} and χ_0^{RPA} are the spin and charge fluctuation RPA susceptibility, respectively. The spin and charge interaction matrix (\bar{U}^s , \bar{U}^c) are the same as in ref. 10. The pairing strength function is

$$\lambda[g(k)] = - \frac{\sum_{ij} \oint_{C_i} \frac{dk_{\parallel}}{v_F(k)} \oint_{C_j} \frac{dk'_{\parallel}}{v_F(k')} g(k) \Gamma_{ij}(k, k') g(k')}{(2\pi)^2 \sum_i \oint_{C_i} \frac{dk_{\parallel}}{v_F(k)} [g(k)]^2}, \quad (12)$$

where $v_F(k) = |\nabla_k E_i(k)|$ is the Fermi velocity on a given Fermi surface sheet C_i . We perform calculations in the spin-rotational invariance case meaning $U' = U - 2J_H$ and $J_H = J'$.

The bare susceptibility and RPA spin susceptibility are shown in Fig. 1(b). The strongest peak is at $(\pi, 0.96\pi)$ which is slightly away from $Q = (\pi, \pi)$. Fig. 3(a) shows the two leading eigenvalues as a function of U at $J_H/U = 0.2$. The dominant pairing symmetry is the $d_{x^2-y^2}$ symmetry with gap nodes along the (π, π) direction. Moreover, the pairing on the $d_{x^2-y^2}$ orbital is much stronger than those on the $d_{xz/yz}$, as shown in Fig. 3(b) at $U = 0.4$. Fig. 3(c) shows the gap function for the subdominant g -wave pairing on the Fermi surfaces. We also perform the calculation on the intra-pocket and inter-pocket pairing strength in the $d_{x^2-y^2}$ -wave pairing. The intra-pocket pairing makes the major contribution. Comparing the gap function on the FS in Fig. 3(b) with the orbital contribution on the FS shown in Fig. 1(a), we can conclude that the intra-pocket pairing is mainly from the $d_{x^2-y^2}$ orbital. The real space Fourier transform of the irreducible singlet vertex $\Gamma_{l_1 l_2 l_3 l_4}(r - r')$, also indicates that the intra-orbital pairing vertex of the $d_{x^2-y^2}$ orbital has the largest negative value on the NN bonds. This means that the $d_{x^2-y^2}$ orbital has the largest attractive interaction on the NN bonds. From these analysis

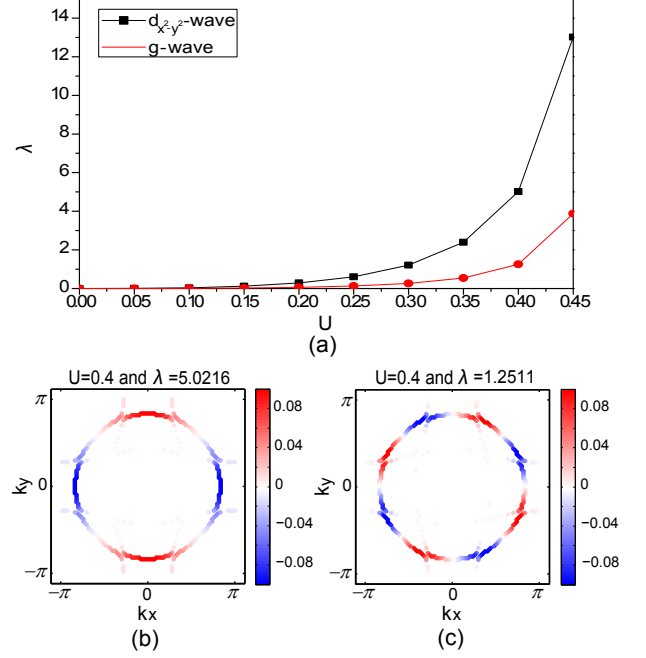


FIG. 3: (color online) The pairing strengths and gap functions for $J_H/U = 0.2$. The two largest pairing strengths as a function of U in (a). The two dominant gap functions for $d_{x^2-y^2}$ -wave(b) and g -wave(c) at $U = 0.4$.

on both the momentum space and real space, the RPA suggests that the $d_{x^2-y^2}$ orbital plays a dominant role in the process of pairing. These results are consistent with the mean field calculation with a small J value in the previous section.

IV. FRG ANALYSIS

In this section, a FRG analysis is performed to analyze the possible SC phase for the Hamiltonian in Eq. 9. The FRG method has been applied to obtain pairing symmetries in both cuprates and iron-based superconductors^{11,12}. It is a very powerful method to analyze the various competing order tendencies in a system.

The detailed description of the method can be found in ref. 13–15. Here we take the band basis and make the Fourier transformation to rewrite the interaction in the momentum space. The interaction part at different flowing parameter Λ is given by

$$H_{int}^\Lambda = \sum_{\mathbf{k}_1, \dots, \mathbf{k}_4} \sum_{n_1, \dots, n_4} \left\{ V_\Lambda^B(n_1, \mathbf{k}_1; n_2, \mathbf{k}_2; n_4, \mathbf{k}_4; n_3, \mathbf{k}_3) \right. \\ \left. \times c_{n_1; \mathbf{k}_1}^\dagger c_{n_2; \mathbf{k}_2}^\dagger c_{n_4; \mathbf{k}_4} c_{n_3; \mathbf{k}_3} \right\} \quad (13)$$

where n_1 to n_4 are the band index and V_Λ^B is the interaction strength. Different competing order tendencies can be characterized by the instability of the corresponding channels. Taking the superconductor order

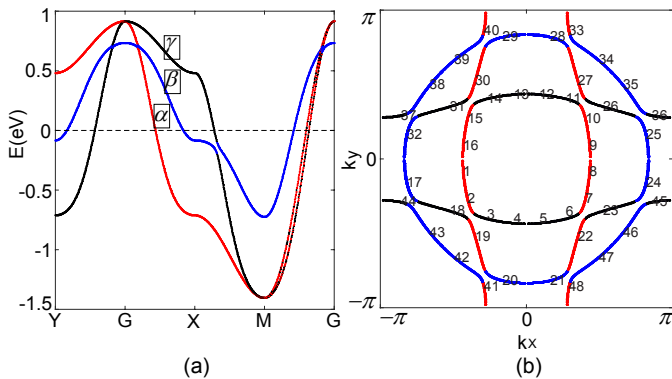


FIG. 4: (color online) The division of the Fermi surfaces used in the FRG calculations with $N=48$.

		$U = 2eV$			$U = 4eV$			
(a,b)		α	β	γ	(a,b)	α	β	γ
α		-0.00	-4.96	-0.59	α	-0.00	-11.49	-1.21
β		-4.96	-168.48	-3.93	β	-11.49	-146.29	-7.24
γ		-0.59	-3.93	-5.93	γ	-1.21	-7.24	-3.62

TABLE I: The leading eigenvalues of scattering vertex of superconducting channel between intra and inter-pockets in $(U, J_H/U) = (2, 0.2)$ and $(4, 0.2)$ respectively near half filling.

parameter $\hat{O}_{\mathbf{k}} = c_{-\mathbf{k},\downarrow}c_{\mathbf{k},\uparrow}$ as an example, we can write it as $\sum_{\mathbf{k},\mathbf{p}} V_{\Lambda}^{SC}(\mathbf{k}, \mathbf{p}) \hat{O}_{\mathbf{k}}^{\dagger} \hat{O}_{\mathbf{p}}$. V^{SC} is decomposed into $V_{\Lambda}^{SC}(\mathbf{k}, \mathbf{p}) = \sum_i w_i(\Lambda) f_i^*(k) f_i(p)^{12,16}$. The leading instability corresponds to the minimum $w_i(\Lambda)$. Its symmetry information is provided by $f_i(p)$.

We divide the FS into $N=48$ patches as shown in Fig. 4(b). In Fig. 5, we report the FRG results near half filling with $J_H/U = 0.2$ and U is chosen as $2eV$ and $4eV$ respectively. The leading instability is a d wave SC order. The pairing gap function $f(\mathbf{k})$ as shown by Fig. 5 has the largest weight in the β band, which suggests that the pairing is orbital selective with dominant pairing on $d_{x^2-y^2}$ orbital. This result is consistent with the RPA calculation. FRG methods are highly sensitive to the density state on FS. The β band hosts a von Hove singularity near half filling while the other two bands, α and γ , have large Fermi velocity near the Fermi level. All these factors result in a dominant pairing in the β band.

We can further check the pairing vertex $V^{SC}(k, p)$ at the final stage. We can compare the values of the elements of the vertex. These elements with large values in this case exactly distribute on the β band. We can also compare the intra and inter pocket contribution to pairing. The scattering vertex of SC channel between intra and inter-pockets can be specified as $V_{a \rightarrow b}^{SC}(b, \mathbf{k}; a, \mathbf{p}) = V_f^B(b, \mathbf{k}; b, -\mathbf{k}; a, \mathbf{p}; a, -\mathbf{p})$ where the symbol a is the pocket index and f means the final stage calculations. Decomposing these scattering vertex into different form factors, we list the leading eigenvalues in Tab.I. The scattering is dominated by the scattering within the β pocket. This $d_{x^2-y^2}$ orbital selective pair-

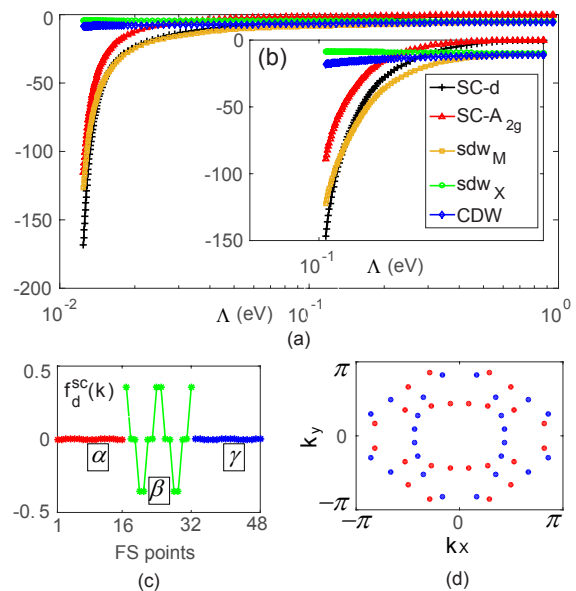


FIG. 5: (color online) The FRG flow and the form factor of the superconducting order. (a-b): The flows of different competing orders in the $(U, J_H/U) = (2, 0.2)$ and $(4, 0.2)$ near half filling. The leading instability in both graphs is the d -wave superconducting order. sdw_X and sdw_M is the spin density wave with propagating \mathbf{Q} vector $(0, \pi)$ and (π, π) respectively. (c): The form factors of leading instability of the superconducting order in the momentum space in the $(U, J_H/U) = (2, 0.2)$. (d) The sign distribution of the d -wave superconducting order on the Fermi surfaces in which the red and blue filled circles represent the positive and negative sign of the pairing order respectively.

ing is very similar to the case in Sr_2RuO_4 ¹⁷ in which the pairing is mainly from d_{xy} ^{18,19} in FRG calculations. Interestingly, similar type of orbital selection occurs and is indicated explicitly on possible superconductivity in $LaOCrAs$ ²⁰. The form factor $f(\mathbf{k})$ in the β pocket can be factorized to $A(\mathbf{k})(\cos(k_x) - \cos(k_y))$ where the $A(\mathbf{k})$ is the momentum-dependent amplitude, and it shares the same symmetry as the $d_{x^2-y^2}$ wave. The A_{2g} -wave which changes sign under the mirror operation about the high symmetry lines is close to the d -wave when $U = 2eV$ while it fades away slightly when $U = 4eV$. This model also reveals the strong spin density wave (SDW) tendency in (π, π) direction labeled by sdw_M as illustrated in Fig. 5(a-b).

The FRG result in the heavy electron doping region is reported in Fig. 6, which is corresponding to near a doping level with one additional electron per site from the half filling. Namely, it is about one third electron doping for each t_{2g} orbital. The interaction parameter here we use is $(U, J_H/U) = (3, 0.1)$. As manifested by Fig. 6(a), the SC channel is not the leading instability any more, and the SDW channel with wavevector (π, π) (sdw_M) arises.

(a,b)	α	β	γ
α	-2.44	-2.20	-2.04
β	-2.20	-4.01	-7.87
γ	-2.04	-7.87	-114.05

TABLE II: The leading eigenvalues of scattering vertex of sdw_M between intra and inter-pockets in electron doping 1 when $(U, J_H/U) = (3, 0.1)$.

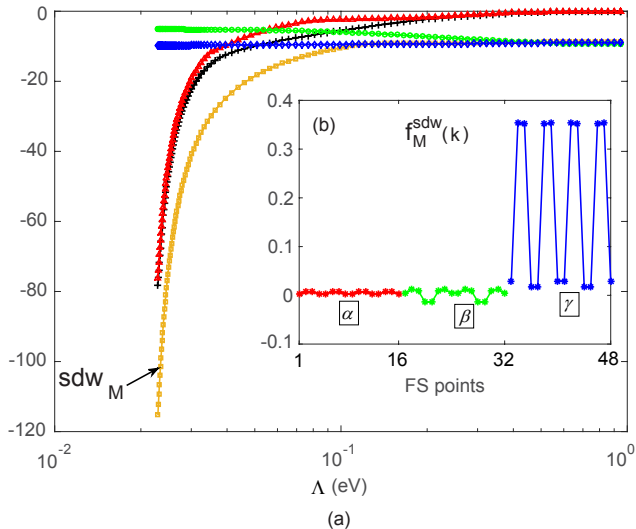


FIG. 6: (color online) (a) The flows of different competing order in $(U, J_H/U) = (3, 0.1)$ when δ is 1. The leading instability is the sdw_M state. (b) The form factor of the sdw_M state.

The sdw_M stems from the nesting on Fermi surfaces between points 43 to 34 as shown in Fig. 4. The form factor $f_M^{sdw}(\mathbf{k})$ of sdw_M is illustrated in Fig. 6(b). The weights of the form factor are located at the γ pocket. More precisely, the largest weights are distributed at the \mathbf{k} points in the γ pocket along the diagonal lines. In our Fermi surface patches, these points are located at 34 – 35 and their counterparts under the C_4 symmetry. We can define the scattering vertex of sdw_M between pockets as $V_{a \rightarrow b}^{sdw_M}(b, k; a, p)$ and decompose it into different form factors as before. The leading eigenvalues are given in the Tab.II. From the Tab.II, the scatterings in the sdw_M channel are attributed to the γ pocket and the contributions from others are very small.

V. DISCUSSION AND CONCLUSION

In summary, we have shown that the d -wave superconducting state is a robust superconducting state in this

family of materials. If we treat this system in a weak interaction region, the superconducting pairing is dominated by the intraorbital pairing of the $d_{x^2-y^2}$ orbital. The $d_{xz, yz}$ orbitals have very small contribution. However, in the strong correlation region, as the bare electron bands are strongly renormalized, all three t_{2g} orbitals can have strong superconducting pairing.

These results suggest that the new materials can serve a bridge to connect cuprates and iron-based superconductors to solve unconventional high T_c mechanism and can be a ground to test the validity of theoretical methods. In cuprates, the electronic physics is governed by the single e_g $d_{x^2-y^2}$ orbital. The d -wave pairing symmetry was obtained by all methods based on repulsive interactions^{8,21,22}. Thus it is difficult to distinguish different theoretical methods. In the new materials, the t_{2g} $d_{x^2-y^2}$ essentially plays the same role as the $d_{x^2-y^2}$ orbital in cuprates. However, the difference among three t_{2g} orbitals can directly distinguish different methods based on strong and weak correlations. Both FRG and RPA, which essentially are only valid in weak interaction region, consistently predict an strongly orbital selective superconducting state. Thus measuring the superconducting gaps on the FSs attributed to the $d_{xz, yz}$ orbitals can determine the validity of these conventional theoretical approaches.

The superconducting pairing mechanism in iron-based superconductors has also become very controversial^{5,23–27}. These new materials have the same multi-orbital electronic physics locally as iron-based superconductors. Because of the difference on their Fermi surface topologies near half filling, the comparison between these two systems can help us to establish general principles in determining superconducting pairing symmetry and pairing mechanisms.

VI. ACKNOWLEDGEMENTS

The work is supported by the Ministry of Science and Technology of China 973 program (No. 2015CB921300), National Science Foundation of China (Grant No. NSFC-1190020, 11534014, 11334012), and the Strategic Priority Research Program of CAS (Grant No.XDB07000000). QHW also acknowledges the supports by the NSFC funding No.11574134.

* these authors contributed equally to this work

† Electronic address: jphu@iphy.ac.cn

¹ J. G. Bednorz and K. A. Muller, Z. Phys. B **64**, 189 (1986).

² Y. Kamihara, T. Watanabe, M. Hirano, and H. Hosono, J.

- Am. Chem. Soc. **130**, 3296 (2008).
- ³ J. P. Hu, C. C. Le, and X. X. Wu, Phys. Rev. X **5**, 041012 (2015).
- ⁴ J. P. Hu, Sci. Bull. **61**, 561 (2016).
- ⁵ J. P. Hu and J. Yuan, Front. Phys. **11**, 117404 (2016).
- ⁶ J. P. Hu and C. C. Le, Sci. Bull. **62**, 212 (2017).
- ⁷ J. P. Hu and H. Ding, Sci. Rep. **2**, 381 (2012).
- ⁸ G. Kotliar and J. L. Liu, Phys. Rev. B **38**, 5142 (1988).
- ⁹ K. J. Seo, B. A. Bernevig, and J. P. Hu, Phys. Rev. Lett. **101**, 206404 (2008).
- ¹⁰ A. F. Kemper, T. A. Maier, S. Graser, H. P. Cheng, P. J. Hirschfeld, and D. J. Scalapino, New J. Phys. **12**, 073030 (2010).
- ¹¹ J. Yuan and J. P. Hu, Europhys. Lett. **113**, 67005 (2016).
- ¹² H. Zhai, F. Wang, and D. H. Lee, Phys. Rev. B **80**, 180505 (2009).
- ¹³ M. Salmhofer, C. Honerkamp, Prog. Theor. Phys. **105**, 135 (2001).
- ¹⁴ W. Metzner, M. Salmhofer, C. Honerkamp, V. Meden, K. Schönhammer, Rev. Mod. Phys. **84**, 299 (2012).
- ¹⁵ C. Platt, W. Hanke, and R. Thomale, Adv. Phys. **62**, 453562 (2013).
- ¹⁶ R. Thomale, C. Platt, W. Hanke, and B. A. Bernevig, Phys. Rev. Lett. **106**, 187003 (2011).
- ¹⁷ A. P. Mackenzie and Y. Maeno, Rev. Mod. Phys. **75**, 657 (2003).
- ¹⁸ Y. Maeno, S. Kittaka, T. Nomura, S. Yonezawa, and K. Ishida, J. Phys. Soc. Jpn. **81**, 011009 (2012).
- ¹⁹ Q. H. Wang, C. Platt, Y. Yang, C. Honerkamp, F. C. Zhang, W. Hanke, T. M. Rice, and R. Thomale, Europhys. Lett. **104**, 17013 (2013).
- ²⁰ W. S. Wang, M. Gao, Y. Yang, Y. Y. Xiang and Q. H. Wang, arXiv:1701.06002 (2017).
- ²¹ D. J. Scalapino, E. Loh, Jr. and J. E. Hirsch, Phys. Rev. B **34**, 8190 (1986).
- ²² F. C. Zhang, C. Gros, T. M. Rice, and H. Shiba, Supercond. Sci. Technol. **1**, 36 (1988).
- ²³ A. V. Chubukov, Annul. Rev. Cond. Mat. Phys. **3**, 57 (2012).
- ²⁴ F. Wang and D. H. Lee, Science **322**, 200 (2011).
- ²⁵ I. I. Mazin and J. Schmalian, Physica C **469**, 614 (2009).
- ²⁶ I. I. Mazin, Nature **464**, 183 (2010).
- ²⁷ P. J. Hirschfeld, M M Korshunov, and I. I. Mazin, Rep. Prog. Phys. **74**, 124508 (2011).